BNL-34316

R 807 note 397
M.A. 12.9.1983

Particle ratios at high transverse momentum in pp collisions at $\sqrt{s}$ = 63 GeV and correlations between high p_T identified charged particles and associated identified charged particles.

The Axial Field Spectrometer Collaboration

T.Akesson[4],M.G.Albrow[10],S.Almehed[6],R.Batley[4],O.Benary[11],H.Bøggild[5], O.Botner[5],H.Breuker[4],H.Brody[7],V.Burkert[1],A.A.Carter[9],J.R.Carter[3], P.Cecil[3],W.Cleland[8],D.Cockerill[10],S.Dagan[11],E.Dahl-Jensen[5], I.Dahl-Jensen[5],P.Dam[5],G.Damgaard[5],W.M.Evans[10],C.W.Fabjan[4],P.Frandsen[5], S.Frankel[7],W.Frati[7],M.D.Gibson[10],U.Goerlach[4],H.Gordon[2],A.Hallgren[4], K.H.Hansen[5],V.Hedberg[6],J.W.Hiddelston[10],H.J.Hilke[4],J.E.Hooper[5], G.Jarlskog[6],P.Jeffreys[10],T.Jensen[4],T.Killian[2],R.Kroeger[8],K.Kulka[6], Jv.d.Lans[4],J.Lindsay[4],D.Lissauer[11],B.Lörstad[6],T.Ludlam[2],A.Markou[4], N.A.McCubbin[10],U.Mjörnmark[6],W.Molzon[7],R.Møller[5],B.S.Nielsen[4],A.Nilsson[6], L.H.Olsen[4],Y.Oren[11],L.Rosselet[4],E.Rosso[4],A.Rudge[4],R.H.Schindler[4], I.Stumer[2],M.Sullivan[8],G.Thorstenson[6],E.Vella[7],J.Williamson[10], W.J.Willis[4],M.Winik[2],W.Witzeling[4],C.Woody[2] and W.A.Zajc[7]

BNL--34316

DE84 010512

1) Physikalisches Institut, Universität Bonn, BRD.
2) Brookhaven National Laboratory, Upton, NY, USA
3) Cambridge University, Cambridge, UK
4) CERN, Geneva, Switzerland.
5) Niels Bohr Institute, Copenhagen, Denmark
6) University of Lund, Sweden
7) University of Pennsylvania, Philadelphia, PA, USA.
8) University of Pittsburgh, PA, USA.
9) Queen Mary College, London, UK.
10) Rutherford Appelton Laboratory, Didcot, UK.
11) University of Tel Aviv, Israel.

Contribution to the International Europhysics Conference on High Energy Physics.
Brighton (UK), 20-27 July 1983

Abstract:

The production of identified charged particles in pp collisions at $\sqrt{s}$ = 63 GeV with an identified high p_T trigger particle emitted in the central region is studied. The measurements were performed at the CERN ISR using the Axial Field Spectrometer. Trigger particle ratios, $\sigma(\pi^{\pm})/\sigma(\text{all}^{\pm})$, $\sigma(K^{\pm})$ and $\sigma(p^{\pm})/\sigma(\text{all}^{\pm})$ are presented for p_T from 5 GeV/c to 8 GeV/c. In addition $\sigma(\pi^{\pm})/\sigma(\text{all}^{\pm})$ is presented in the p_T region from 2.5 GeV/c to 4.5 GeV/c.

The charge compensation in the hemisphere containing the trigger particle is shown to depend strongly on the identity of the trigger particle and on the identity of the associated particles.

Introduction

We report on measurements of identified charged particles produced in pp collisions at the c.m.s. energy $\sqrt{s}$ = 63 GeV with an identified high p_T charged trigger particle emitted in the central region, with rapidity less than about 0.8.

It is well established that in general such collisions give rise to a 4-jet structure |1, 2|. In the hemisphere containing the high p_T trigger particle other particles of moderately high p_T are closely collimated around the trigger particle direction. In the opposite hemisphere (the away side) high p_T-particles are well collimated in azimuth opposite to the trigger direction, but form, statistically, a broad enhancement in rapidity as the rapidity of the recoil jet varies from collision to collision.

We first present the ratios $\sigma(\pi^{\pm})/\sigma$(all charged particles) in the p_T interval from 2.5 GeV/c to 4.5 GeV/c and the ratios $\sigma(\pi^{\pm})$, $\sigma(K^{\pm})$, $\sigma(p^{\pm})/\sigma$(all charged particles) in the p_T interval from 5 GeV/c to 8 GeV/c. Such ratios or the cross sections separately have earlier been measured only at lower $\sqrt{s}$ or at lower p_T |3, 4| apart from a measurement by the CDHW collaboration of the ratio of charged pions to all charged particles at the same $\sqrt{s}$ and approximately the same p_T range but at a c.m.s. angle of 50° |5|.

Next we study the charge correlations between the identified high p_T particle and associated identified charged particles. Similar measurements have been reported by the CDHW collaboration |1| and the BFS collaboration |2a|. However, in most cases the associated particles were unidentified.

The correlations on the trigger side are much influenced by the presence of resonances, but in evaluating the charge correlation for different particle identities we can study effects due to the quark fragmentation. As fragmentation is a soft process the primary quark is likely to be found in the high p_T trigger particle, giving rise to a particular correlation pattern. Our results will be compared with a Monte Carlo model, the so-called Lund model |6|, where the parton-parton interactions are calculated in perturbative QCD to order α_s^2 taking care of color string configurations. These color strings then fragment in the way observed in e^+e^- interactions. Some of the different collisions at the parton level will also lead to long range correlations between the triggering particle and the fast particles on the away side.

Apparatus and data analysis

The experiment was performed at the CERN ISR using the Axial Field Spectrometer, shown in Fig. 1 in a view transverse to the colliding beams. The apparatus and its performance are described in detail elsewhere [7]. Here we mention briefly only those components of the apparatus which were used in the present investigation.

The central cylindrical drift chamber is 1.4 m long and extends radially from 0.2 to 0.8 m. It is segmented azimuthally in 4° sectors each with 42 sense wires. In azimuth it provides a full 2π coverage except for two 16° wedges above and below the interaction region. It is situated in an axially symmetric magnetic field of $\sim$0.5 T. Position coordinates in the plane transverse to the sense wires are determined by the drift time and have a resoluti of $\sim$230 μm. Along the wires, parallel to the beams, the position is measured by relative pulse height measurements at the two ends of the wires. The corresponding resolution is $\sim$1.5 cm. The pulse height measurements also provide dE/dx information, used for partic identification. This gives π identification in the momentum range of 0.2 to 0.5 GeV/c and K identification in the momentum range 0.3 to 0.7 GeV/c and baryon identification in the momentum range 0.4 to 1.3 GeV/c.

Three sets of threshold Cerenkov counters subtend an azimuthal angle of 45° and $45° < \theta < 135°$ in polar angle. The one closest to the drift chamber, the aerogel Cerenkov counter, consist of 88 cells arranged in 4 layers in depth. The cells are read out using wave length shifter technique. The average number of photo-electrons per cell produced by a $\beta \sim 1$ particle is only 0.3 as determined from the data, resulting in an efficiency/track of aroun 2/3 for having at least 1 signal from the aerogel counter. On the other hand 15% of the tracks with momentum below the π threshold (0.5 GeV/c) have associated noise in the counter. In this study th aerogel counter is used to identify π-mesons and in the momentum range of 0.5 to 2 GeV/c to purify the identification of heavy parti by comparison with the information from the dE/dx and the high pressure Cerenkov counter.

The second Cerenkov counter, the high pressure counter, is subdivided into 12 optical cells. The average number of photo-

electrons produced by a $\beta\sim1$ particle is $\sim$20. This allows pion/heavy particle separation for $1.5<p<5.5$ GeV/c. After appropriate cuts the identified heavy particle sample is quite clean, whereas the pion sample has a contamination of heavier particles of $\sim$1.5%, mainly due to γ-conversions from overlapping π^0 decays.

The third Cerenkov counter is an atmospheric pressure counter consisting of 18 optical cells. The average number of photoelectrons for a $\beta\sim1$ particle is $\sim$10. Together with the high pressure counter it provides pion, kaon and proton separation for $p > 5.5$ GeV/c.

Copper calorimeters placed behind the atmospheric pressure counters cover 1/7 of the solid angle of these counters. They were installed to provide a cross-check of the momentum measurement at $p>8$ GeV/c and were also used in the trigger for part of the data sample.

Interactions resulting in the production of a high p_T charged particle within the solid angle of the Cerenkov counters were selected using a three level trigger. The first level uses a scintillator hodoscope surrounding the beam pipe together with groups of wires in the PWC's to require $p_T>0.8$ GeV/c. The second level uses hits in individual wires of the PWC's , and the last level uses a microprocessor operating on the appropriate drift chamber signals. For details see ref. [8].

The events were first processed through the AFS drift chamber reconstruction and fitting programs [9]. Events were accepted if they contained a reconstructed primary vertex, a condition fulfilled by 99% of the events. Cuts were imposed on the tracks to ensure that they belonged to the event and that their momenta were reasonably well determined. All tracks were transformed to the c.m.s., using a pion mass if not identified. Cuts on associated particles restricted them to be within $\pm$0.8 in rapidity and within $0.3<p_T<5$ GeV/c. No corrections have been applied for the gaps up and down or for a somewhat reduced acceptance for $|y|>0.6$. Also no corrections have been applied for a reduced efficiency for tracks crossing the trigger track. That loss was found to be $\sim$15% inside an angle of 10° to the trigger track. Data were collected with both polarities of the magnetic field. No significant differences were found for different magnet polarities. The acceptance of the associated particles is thus charge independent Tracks within the acceptance of the Cerenkov counters were refitted

using both the drift chamber information and the reconstructed space points in the PWC's. This procedure served to reject false high p_T tracks, to reject particles interacting in the material of the Cerenkov counters and to improve the momentum resolution to approximately $\Delta p/p \sim 10\%$ at p=10 GeV/c.

Particle ratios

Fig.2 and Fig.3 show as a function of p_T for positively and negatively charged particles, respectively, the fractional composition of the trigger particle flux into pions and heavier particles (for $p_T < 5$ GeV/c) and into pions, kaons and protons (for $p_T > 5$ GeV/c). The ratios are averages over the c.m.s. polar angle interval from 45° to 135° with $\langle\theta\rangle = 90°$ and $\sigma(|\theta - 90°|) \cong 20$. Within our statistics we see no variation in the ratios with θ. For comparison we also show on Fig.2 and 3 the ratios (between invariant cross sections) measured by the CDHW collaboration [5] at $\langle\theta\rangle = 50°$, and the extrapolation of the fit made by the BS collaboration to their data at lower p_T and/or lower $\sqrt{s}$ (Table 4, ref. 4).

The ratios have been corrected for contamination of the pion sample by heavier particles (a correction to the ratios of 1.5% for $p_T<5$ GeV/c), for nuclear absorption and decays (corrections of 0.5 - 3%) and for a slightly worse acceptance for protons than for pions and kaons at $p_T>5$ GeV/c (corrections $\sim$1%). The errors on Figs.2 and 3 are statistical errors only. The systematic errors are estimated to be everywhere less than the statistical errors.

For positively charged particles we find the same pion ratio as the CDHW collaboration over the whole p_T range. For negatively charged particles the pion ratios are again equal at

$p_T < 5$ GeV/c but we do not observe the rise in the ratio found by the CDHW collaboration at higher values of p_T. This may be an indication that heavy negatively charged particles are more centrall produced than π^-'s at very high p_T.

The Lund model with the choice of parameters given in |6| does not reproduce the data very well. In the model the ratios are independent of p_T over the range from 3 GeV/c to 7 GeV/c giving the ratios 0.7, 0.15, 0.15 for π^-, K^-, and $\bar{p}$ and the ratios 0.65, 0.175 0.175 for π^+, K^+ and p.

Charge compensation

We will now investigate how the charge of a fast particle in the trigger side jet is compensated in different regions of the phase space. A similar study has been performed by the CDHW collaboration at the CERN ISR |1|. Here we will study the charge compensation along an axis given by the direction of the trigger sid jet. Our approach follows that given by the TASSO |10| and PLUTO |11| collaborations at PETRA.

The trigger side jet axis is found by a jet algorithm |12| using the charged particles with a $p_T > 0.3$ GeV/c. This axis is, within a few degrees, given by the trigger particle. We define an asymmetry $A(y,y')=2P(y,y')-1$ where $P(y,y')$ is the probability of finding opposite charges for two given particles located at rapiditi y and y' along the jet axis (for zero charge compensation P is equal to 0.5 and A is zero). We will study the quantity $\bar{A}(y)=\int_2^5 A(y,y')\rho(y,y')dy' / \int_2^5 \rho(y,y')dy'$ which is obtained by weighti the asymmetry $A(y,y')$ with the two particle density $\rho(y,y')$ and averaging over all fast particles in the high rapidity interval $2 \leq y' \leq 5$. $\bar{A}(y)$, ranging between +1 and -1, measures the strength of the charge compensation which acts between the average pair of particles, the fast particle at y' and the other one at y.

Fig.4 shows the general behaviour of the charge compensation as a function of rapidity along the jet-axis, for all negativ and positive particles regardless of their identity. There is a strong short range correlation and a much weaker long range correlation: both are stronger for fast particles of negative charge. However, the charge compensation when the second particle is a π has the same strength for both charges of the fast particle, Fig.5a, but a clear difference in charge compensation is seen then where the second particle is a heavy particle (h), see Fig.5b. In Fig.6 we

...last particle and the other is identified.
...teresting effects: fast π^+ particles show much less
... range charge compensation by heavy particles than fast π^-
particles. Fast h^- particles have stronger charge compensation by
other heavy particles than fast h^+ particles.

The interpretation of these effects follows a naive model of quark fragmentation. First we discuss the fast π charge compensated by heavy particles, the majority of which are K-mesons. A fast π^+ contains often a leading valence u-quark which has been combined with a $\bar{d}$-quark from a $d\bar{d}$-quark pair creation. The d-quark can then combine with an $\bar{s}$ from an $s\bar{s}$-quark pair-creation to form a K^o, (it cannot form a K^-) close to the π^+ in rapidity which prevents a short range compensation by K-mesons to the π^+. On the other hand, a fast π^- ($d\bar{u}$) can get a K^+ ($u\bar{s}$) as a close partner giving rise to a short range effect.

Other short range effects come from resonance production ...ut these should be completely symmetric for the π,K case.

The stronger charge compensation for K^-K^+ (leading K^-) ...an for K^+K^- (leading K^+) could stem from the difference that while ...$^+$ ($u\bar{s}$) can be formed from a valence u-quark from the interaction, ...K^- contains no valence quark and will therefore be accompanied ...ne unit of both charge and strangeness.

Using the Lund Monte Carlo |6| we have calculated what ...odel predicts for these effects, see Fig.7, and we see that ...del is in quite good accordance with our data.

...ions

The composition of the charged particle flux around $\Theta = 90°$ ...s has been measured in pp collisions at the cms energy ...eV for transverse momenta up to 8 GeV/c. In the p_T range .../c to 8 GeV/c we find the π^+, K^+, p composition to be about 0.13 and the π^-, K^-, $\bar{p}$ composition to be about 0.10-0.05 (Figs. 2 and 3).

...r the correlations between high p_T identified particles ...d particles we find:

...pensation on the same side as the trigger depends ...e identity of the associated particles and on the iden- ...gger particle. The differences in the correlations ...vely a simple picture of quark fragmentation and the ...duced quantitatively in the Lund Monte Carlo model

References

|1| a) Cern-Dortmund-Heidelberg-Warsaw Collaboration CERN/EP 82-184.

b) Cern-Dortmund-Heidelberg-Warsaw Collaboration CERN/EP 82-212.

c) H.G. Fischer, rapp. talk EPS conference Lisbon.

|2| a) M.G. Albrow et al, Nucl.Phys. B145, (1978) 305.

b) M.G. Albrow et al, Nucl.Phys. B160, (1979) 1.

|3| a) R. Cottrell et al, Phys.Lett. 55B (1975) 341.

b) M. Della Negra et al, Phys.Lett. 59B (1975) 481.

c) D. Antreasyan et al, Phys.Rev.Lett. 38 (1977) 112.

|4| B. Alper et al, Nucl.Phys. 100B (1975) 237.

|5| D. Drijard et al, Nucl.Phys. 208B (1982) 1.

|6| Hans-Uno Bengtsson, LU TP 82-15 and references given therein

|7| a) H. Gordon et al, Nucl.Instr. & Methods 196 (1982) 303.

b) O. Botner et al, Nucl.Instr. & Methods 196 (1982) 315.

|8| B. Heck et al, EPS Conf. on Computing, Bologna 1980.

|9| S. Almehed and B. Lörstad, Comput.Phys.Comm. 27, 1981.

|10| R. Brandelik et al, Phys.Lett. 100B (1981) 357.

|11| C. Berger et al, DESY 82-058.

|12| T. Sjöstrand, Comput.Phys.Comm. 27 (1982) 243.

|13| T. Åkesson et al, Phys.Lett. 118B (1982) 178.

ACKNOWLEDGEMENTS

We acknowledge with thanks the work of the CERN EP, EF and ISR divisions on the construction and installation of the Axial Field Spectrometer. Support from the Research Councils in our home countries is also gratefully acknowledged.

This research has been supported in part by the U.S. Dept. of Energy under Contract No. DE-AC02-76CH00016.

Figure captions

Fig. 1 The Axial Field Spectrometer (view transverse to the collision axis). The magnet coils are in fact out of the plane, on the poles. The left calorimeter wall is shown in a retracted position.

Fig. 2 The fractional composition of the particle flux into pions, kaons and protons, as a function of p_T, for positively charged particles.

Fig. 3 The fractional composition of the particle flux into pions, kaons and antiprotons, as a function of p_T, for negatively charged particles.

Fig. 4 Compensation of charge, $\tilde{A}(y)$, of particles in the test interval $2<y'<5$ (fast particles) as a function of rapidity. -: fast negative particles, x: fast positive particles

Fig. 5 Charge compensation by associated identified particles as a function of rapidity, $\tilde{A}(y)$.
-: fast negative particles, x: fast positive particles from a test interval $2<y'<5$.
a) associated particles identified as pions,
b) associated particles identified as K or $p/\bar{p}$.

Fig. 6 Charge compensation of identified fast particles, $2<y'<5$, by associated identified particles as a function of rapidity, $\tilde{A}(y)$
a) - fast π^- compensated by π:s
x fast π^+ compensated by π:s
b) - fast h^- compensated by π:s
x fast h^+ compensated by π:s
c) - fast π^- compensated by h:s
x fast π^+ compensated by h:s
d) - fast h^- compensated by h:s
x fast h^+ compensated by h:s

Figure captions (cont'd)

Fig. 7 Monte Carlo prediction of charge compensation of identified fast particles, $2<y'<5$, by associated identified particles as a function of rapidity, $\bar{n}(y)$

a) - fast π^- compensated by π:s
   x fast π^+ compensated by π:s
b) - fast h^- compensated by π:s
   x fast h^+ compensated by π:s
c) - fast π^- compensated by h:s
   x fast π^+ compensated by h:s
d) - fast h^- compensated by h:s
   x fast h^+ compensated by h:s

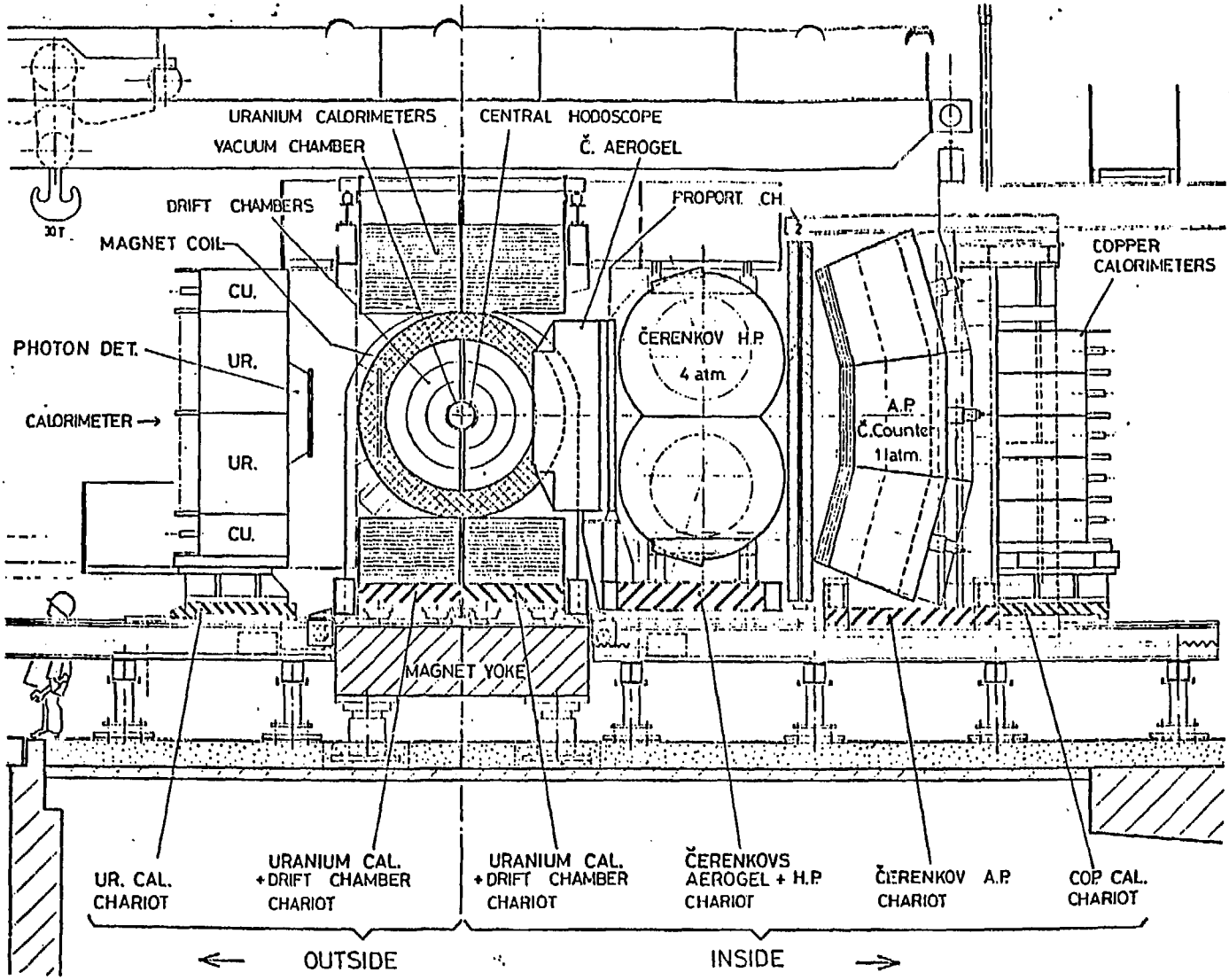
URANIUM CALORIMETERS
VACUUM CHAMBER
CENTRAL HODOSCOPE
Č. AEROGEL
PROPORT. CH.
DRIFT CHAMBERS
MAGNET COIL
30 T.
COPPER CALORIMETERS
CU.
PHOTON DET.
UR.
CALORIMETER
UR.
CU.
ČERENKOV H.P.
4 atm.
A.P.
Č.Counter
1 atm.
MAGNET YOKE
UR. CAL. CHARIOT
URANIUM CAL. + DRIFT CHAMBER CHARIOT
URANIUM CAL. + DRIFT CHAMBER CHARIOT
ČERENKOVS AEROGEL + H.P. CHARIOT
ČERENKOV A.P. CHARIOT
COP. CAL. CHARIOT
OUTSIDE
INSIDE

Fig. 1

Fig. 2

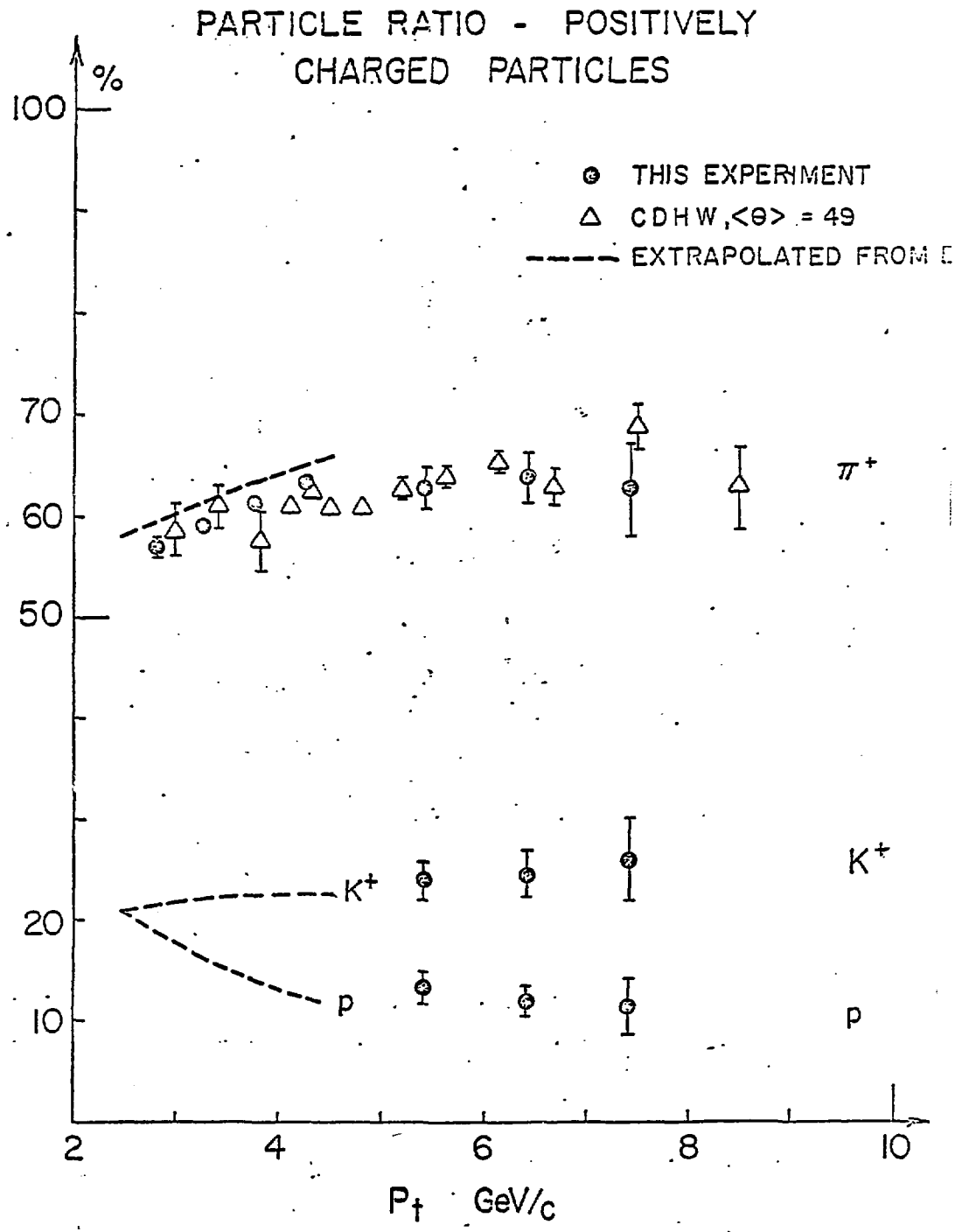
PARTICLE RATIO - POSITIVELY CHARGED PARTICLES
%
100
70
60
50
20
10
THIS EXPERIMENT
CDHW, <θ> = 49
EXTRAPOLATED FROM
π+
K+
p
K+
p
2
4
6
8
10
Pt GeV/c

Fig. 3

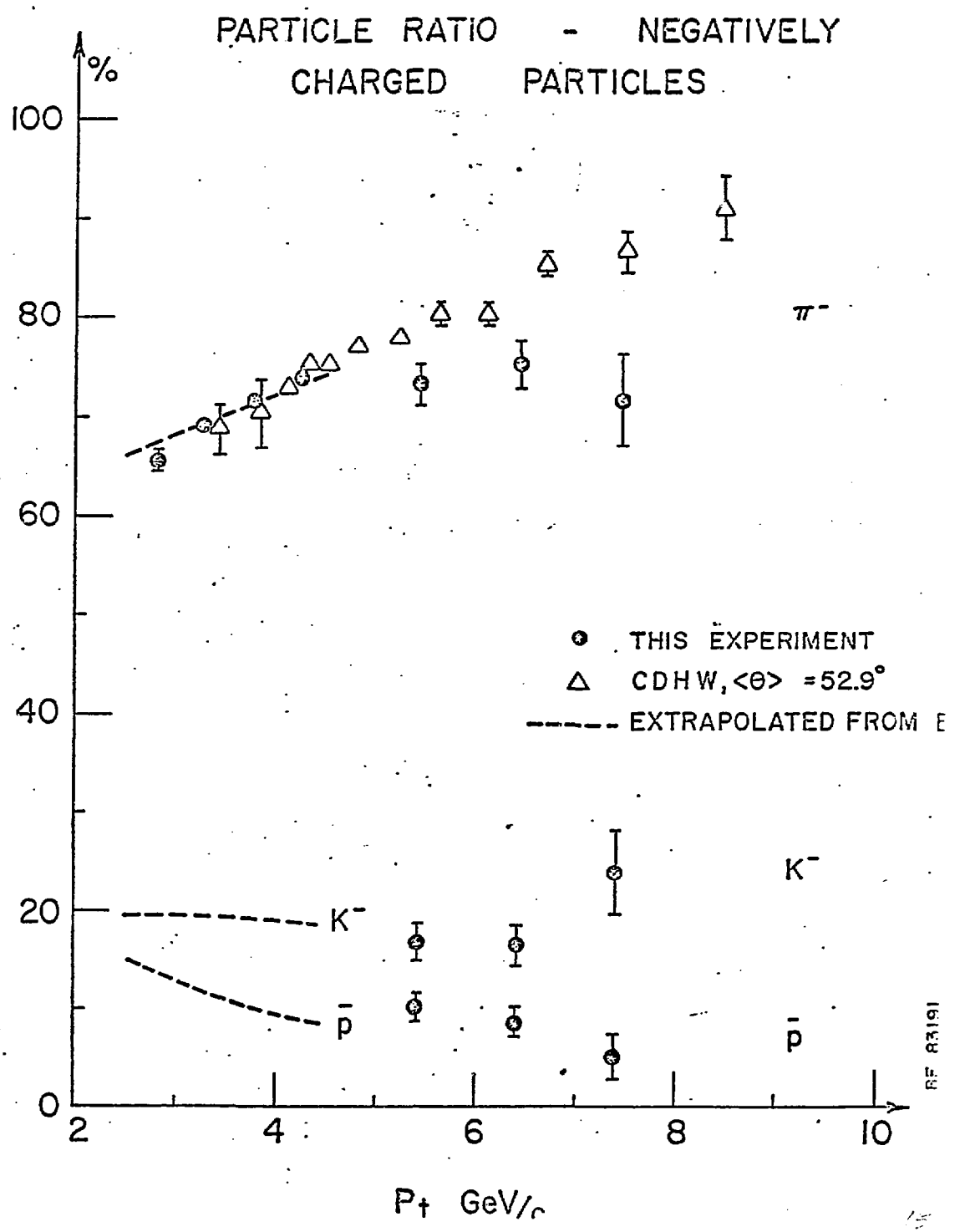
PARTICLE RATIO - NEGATIVELY CHARGED PARTICLES
%
100
80
60
40
20
0
2
4
6
8
10
P_t GeV/c
π^-
K^-
$\bar{p}$
THIS EXPERIMENT
CDHW, <θ> =52.9°
EXTRAPOLATED FROM E
RF 83191

Fig. 4

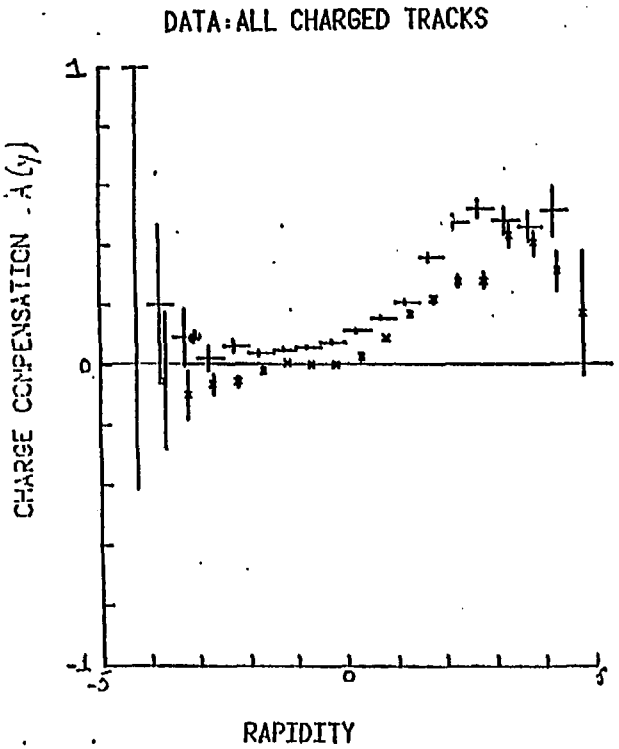
DATA: ALL CHARGED TRACKS
CHARGE COMPENSATION $A(y)$
1
0
-1
-5
0
5
RAPIDITY

Fig. 5

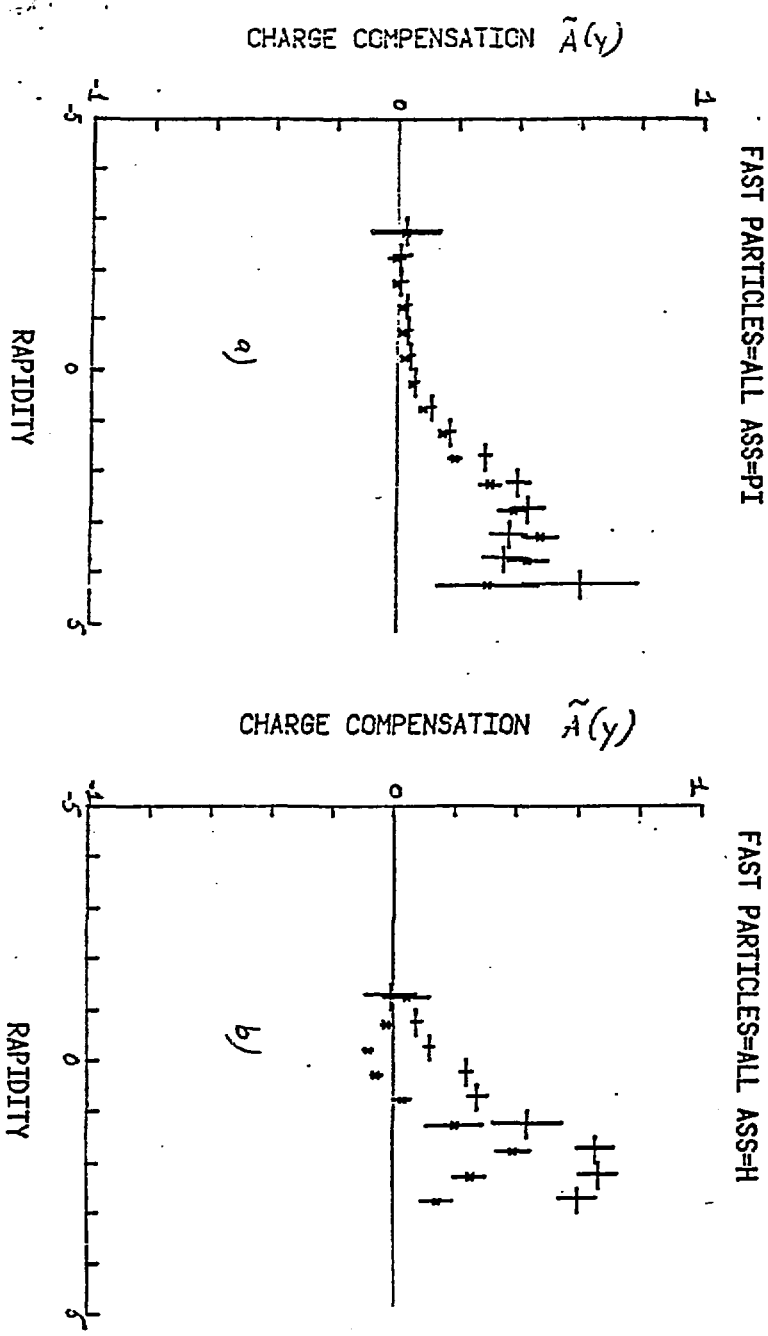
CHARGE COMPENSATION $\tilde{A}(y)$
FAST PARTICLES=ALL ASS=PI
RAPIDITY
-1
-.5
0
.5
1
a)
CHARGE COMPENSATION $\tilde{A}(y)$
FAST PARTICLES=ALL ASS=H
RAPIDITY
b)

Fig. 6 a,b

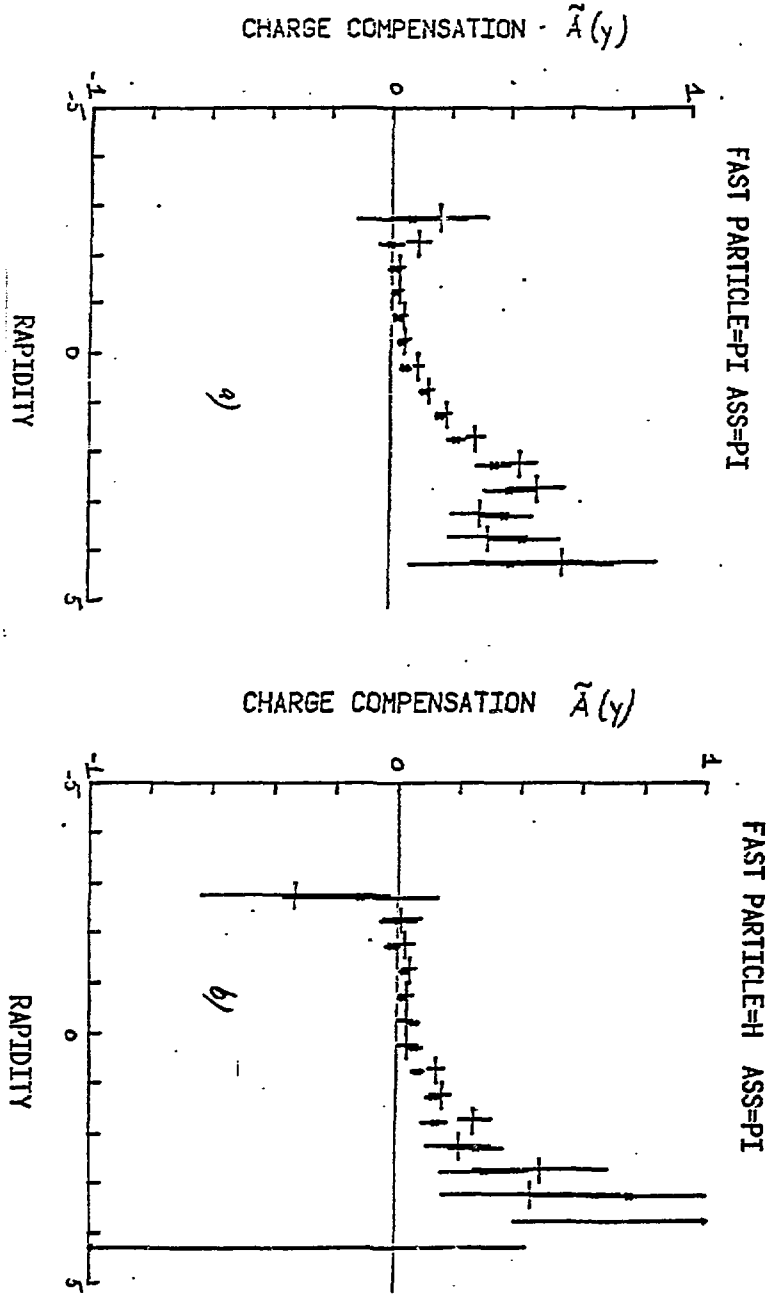
CHARGE COMPENSATION - $\tilde{A}(y)$
-1
-5
0
1
5
RAPIDITY
FAST PARTICLE=PI ASS=PI
a)
CHARGE COMPENSATION $\tilde{A}(y)$
-1
-5
0
1
5
RAPIDITY
FAST PARTICLE=H ASS=PI
b)

Fig. 6 c,d

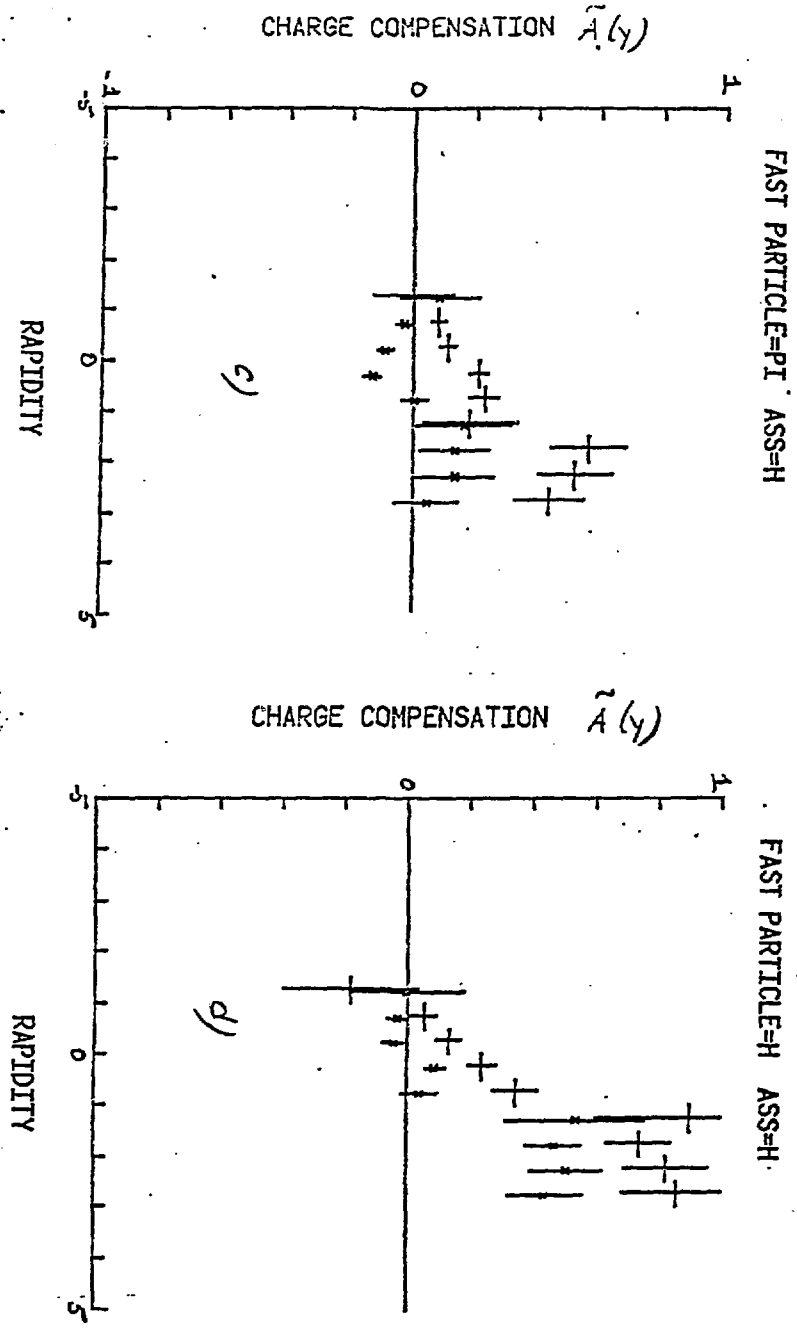
CHARGE COMPENSATION $\tilde{A}(y)$
-1
0
1
-5
0
5
RAPIDITY
FAST PARTICLE=PI ASS=H
c)
CHARGE COMPENSATION $\tilde{A}(y)$
-1
0
1
-5
0
5
RAPIDITY
FAST PARTICLE=H ASS=H
d)

Fig. 7 c,d

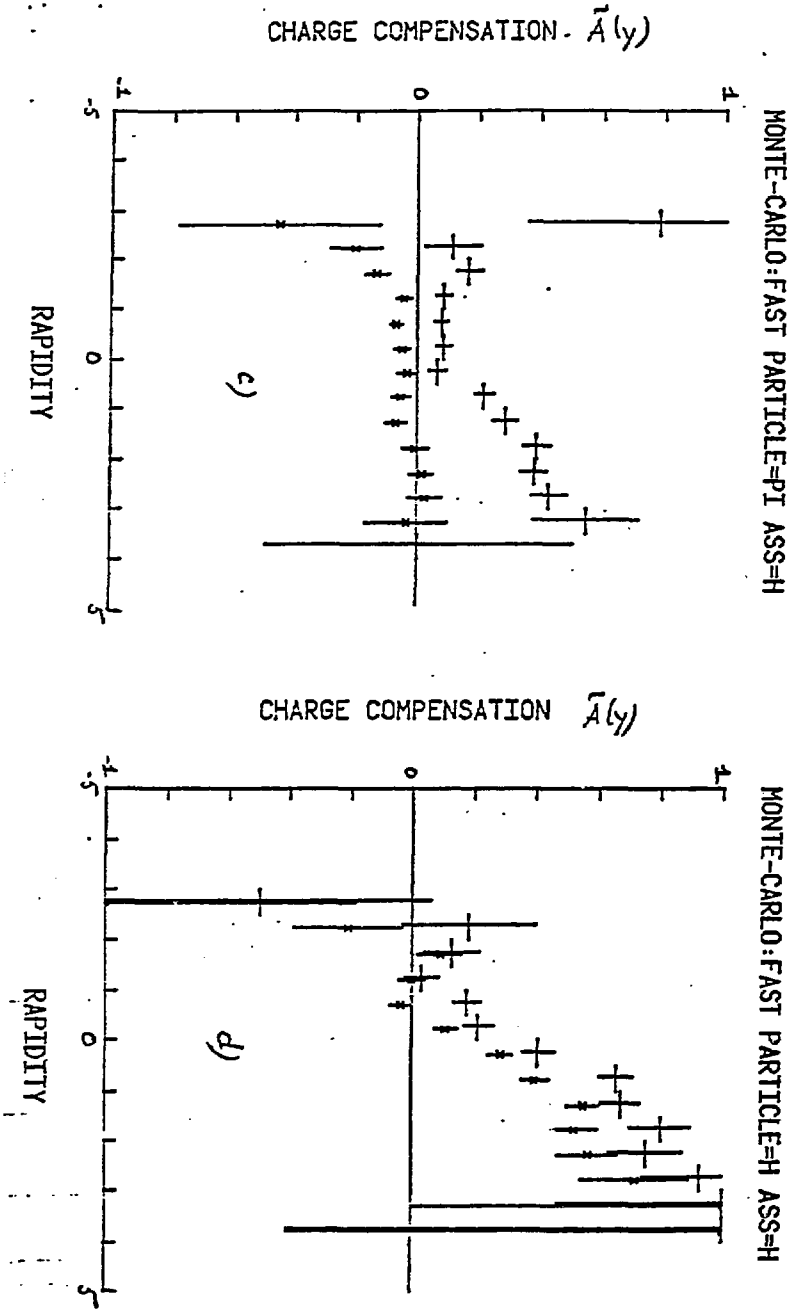
CHARGE COMPENSATION. $\bar{A}(y)$
MONTE-CARLO:FAST PARTICLE=PI ASS=H
RAPIDITY
c)
CHARGE COMPENSATION $\bar{A}(y)$
MONTE-CARLO:FAST PARTICLE=H ASS=H
RAPIDITY
d)

Fig. 7 a,b

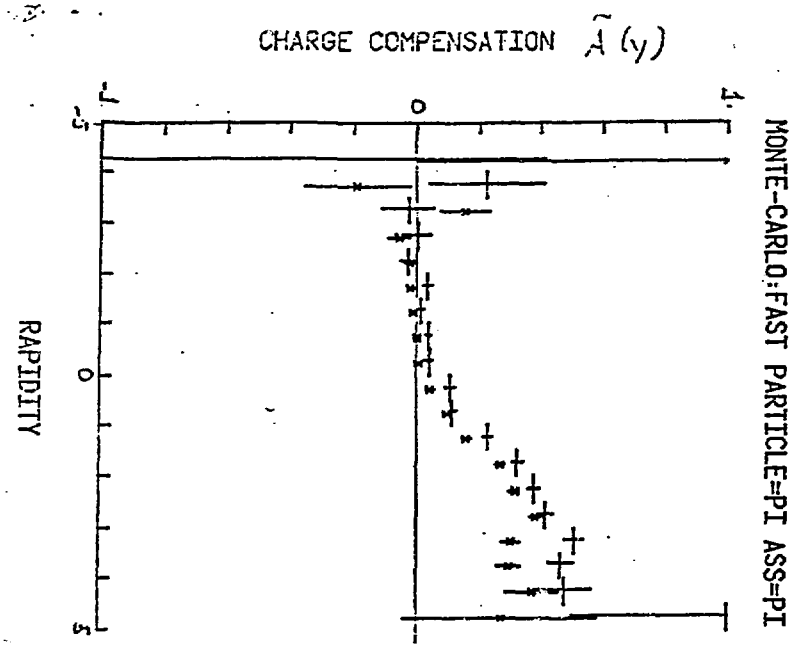
CHARGE COMPENSATION $\tilde{A}(y)$
MONTE-CARLO:FAST PARTICLE=PI ASS=PI
RAPIDITY
-5
0
5

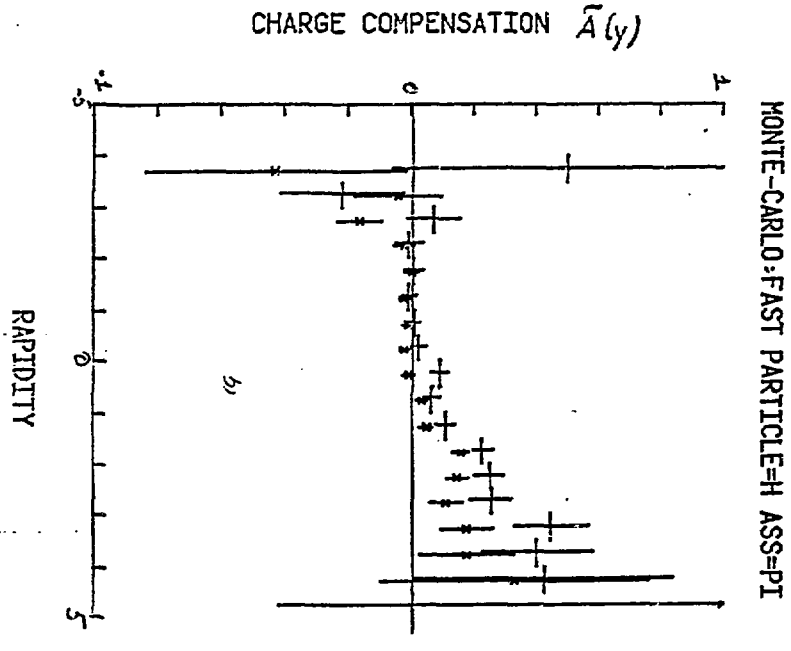
CHARGE COMPENSATION $\tilde{A}(y)$
MONTE-CARLO:FAST PARTICLE=H ASS=PI
RAPIDITY
-5
0
5
b)

DISCLAIMER